14B.13 LARGE-EDDY SIMULATION OF THE STABLE BOUNDARY LAYER: REVISITING GABLS WITH A LINEAR ALGEBRAIC SUBGRID-SCALE TURBULENCE MODEL

Rica Mae Enriquez*[1] and Robert L. Street[2]
[1]University of Cambridge, Cambridge, UK
[2]Stanford University, Stanford, CA

1. INTRODUCTION

The stable boundary layer [SBL] has a more delicate dynamical balance than the neutral or convective boundary layers. Thus, understanding and parameterizing its development has been much slower, and experimental and numerical studies of the SBL are challenging. The thin, cooled surface layer of the SBL is governed by the geostrophic wind and surface cooling. The turbulence is regulated by shear, dissipation, and buoyancy destruction. Two characteristics of the SBL that make numerical studies difficult are: (1) the energetic eddies in the SBL can be smaller than 1 m, so using a domain that is both large enough and resolved enough can be computationally expensive, and (2) the turbulence is anisotropic because stratification inhibits vertical motions. The second factor has led to the development of subgrid-scale [SGS] turbulence models that can provide anisotropy.

In this paper, we investigate the manner in which our Linear Algebraic Subgrid-Scale model (LASS - see Enriquez, 2013) can simulate a cooling SBL. As a prologue, we show how LASS behaves under different cooling fluxes and how it provides appropriate anisotropy. Then, we examine how LASS performs in a moderately stable case, the Global Energy and Water Cycle Experiment Atmospheric Boundary Layer Study [GABLS]. This case is based on Arctic observations, simulated first by Kosović and Curry (2000) and later with a variety of LES turbulence models by Beare et al. (2006).

2. LASS, THE SGS TURBULENCE MODEL

The dry-air dynamics [under the Boussinesq approximation with buoyancy effects and Coriolis forces] and thermodynamics equation set are the basis for the LES; see Enriquez (2013) for details. The SGS terms are given by:

$$A_{ij} = \overline{u_i u_j} - \overline{u}_i \overline{u}_j, \tag{1}$$

$$a_i = \overline{u_i \theta} - \overline{u}_i \overline{\theta}. \tag{2}$$

The SGS model includes production, pressure redistribution, dissipation, and buoyancy generation terms. It is applicable to a range of atmospheric stability conditions for the unsaturated atmosphere [see Enriquez (2013) for LES of the neutral, convective and transitioning boundary layers]. The SGS stresses are solved as a system of linear equations and are fully coupled to the set of equations that model the active SGS heat flux. Thus,

$$0 = -A_{ik}\frac{\partial \overline{u}_j}{\partial x_k} - A_{kj}\frac{\partial \overline{u}_i}{\partial x_k} + \Pi_{ij} - \frac{2}{3}\overline{\varepsilon}\delta_{ij} + \frac{g}{\theta_o}\left(a_i\delta_{j3} + a_j\delta_{i3}\right), \tag{3}$$

$$0 = -A_{ik}\frac{\partial \overline{\theta}}{\partial x_k} - a_k\frac{\partial \overline{u}_i}{\partial x_k} + \Pi_{i\theta}. \tag{4}$$

where

$$\begin{aligned}\Pi_{ij} = & \underbrace{-c_1\frac{\overline{\varepsilon}}{\overline{e}}\left(A_{ij} - \frac{2}{3}\overline{e}\delta_{ij}\right)}_{\text{Slow Pressure-Strain}} \\ & \underbrace{-c_2\left(P_{ij} - \frac{2}{3}P\delta_{ij}\right) - c_3\overline{e}\overline{S}_{ij} - c_4\left(D_{ij} - \frac{2}{3}P\delta_{ij}\right)}_{\text{Rapid Pressure-Strain}} \\ & \underbrace{-c_g\frac{g}{\theta_0}\left(a_i\delta_{j3} + a_j\delta_{i3} - \frac{2}{3}a_3\delta_{i3}\delta_{ij}\right)}_{\text{Buoyant Force}} \\ & \underbrace{+\left(c_5\frac{\overline{\varepsilon}}{\overline{e}}\left(A_{ij} - \frac{2}{3}\overline{e}\delta_{ij}\right) + c_6P_{ij} - c_7D_{ij} + c_8\overline{e}\overline{S}_{ij}\right)f(z)}_{\text{Wall Effects}},\end{aligned} \tag{5}$$

$$\overline{S}_{ij} = \left(\frac{\partial \overline{u}_i}{\partial x_j} + \frac{\partial \overline{u}_j}{\partial x_i}\right), \tag{6}$$

$$D_{ij} = -\left(A_{ik}\frac{\partial \overline{u}_k}{\partial x_j} + A_{jk}\frac{\partial \overline{u}_k}{\partial x_i}\right), \tag{7}$$

$$P_{ij} = -\left(A_{ik}\frac{\partial \overline{u}_j}{\partial x_k} + A_{jk}\frac{\partial \overline{u}_i}{\partial x_k}\right), \tag{8}$$

$$P = -A_{ij}\frac{\partial \overline{u}_j}{\partial x_i}, \tag{9}$$

$$f(z) = 0.27\frac{\Delta_g}{z}. \tag{10}$$

The SGS heat flux pressure redistribution term, $\Pi_{i\theta}$, is modeled similarly:

$$\Pi_{i\theta} = \underbrace{-c_{1\theta}\frac{\overline{\varepsilon}}{\overline{e}}a_i}_{\text{Slow Pressure-Strain}} \quad \underbrace{+c_{2\theta}a_k\frac{\partial \overline{u}_i}{\partial x_k}}_{\text{Rapid Pressure-Strain}} \tag{11}$$

* *Corresponding author address*: Rica Mae Enriquez, University of Cambridge, Department of Applied Mathematics and Theoretical Physics, Cambridge, UK, CB3 0WA; rica@alumni.stanford.edu

P is the generation rate of turbulence energy. The wall function, $f(z)$, is a wall function that relates the local vertical grid scale, Δ_z, with distance from the surface, z, whereas typically $\Delta_g = (\Delta_x\Delta_y\Delta_z)^{1/3}$. Model coefficients are given in Enriquez (2013), and here N is the Brunt-Väisälä frequency while

$$S = |S_{ij}|, \tag{12}$$

$$\bar{\varepsilon} = C_\varepsilon \frac{\bar{e}^{1.5}}{\Delta_B}, \tag{13}$$

$$\Delta_B = \begin{cases} \Delta_g & \text{if } N^2 \le 0, \\ 0.76\sqrt{\dfrac{\bar{e}}{N^2}} & \text{if } N^2 > 0. \end{cases} \tag{14}$$

Here we use a SGS TKE model from Yoshizawa (1986). We modified the TKE model to allow for buoyancy effects. The modification is analogous to the adjustments that allow the Smagorinsky model to account for static stability changes, so

$$\bar{e} = \begin{cases} 0.083\Delta_g{}^2\left(S^2 - N^2/Pr_t\right) & \text{if } N^2 < 0, \\ 0.083\Delta_g{}^2 S^2 & \text{if } N^2 \ge 0, \end{cases} \tag{15}$$

where Pr_t is the turbulent Prandtl number (= ⅓ here).

3. STEP COOLING SIMULTIONS

3.1 *LES Setup*

We simulated the dry stable boundary layer with a constant geostrophic wind of 10 m s^{-1} at a latitude of 43°N. At this latitude, the Coriolis parameter, f, is 10^{-4} s^{-1}. We initialized our simulations with the well-developed neutral boundary layer with a background temperature of 300 K, as described in Enriquez (2013). Following Jiménez and Cuxart (2005), we allowed it to evolve for 100,000 s before we began cooling the surface. Once we began the cooling regime, the surface fluxes were computed with a stability-dependent drag coefficient, using Monin-Obukhov similarity theory and a roughness length of 0.1 m. Additionally, we applied Rayleigh damping above 500 m. Other general parameters of the LES simulations can be found in Table 1.

Domain height, H	640 m
Domain width x length	640 m x 640 m
Reference temperature	300 K
Geostrophic wind	$(U_g, V_g) = (10, 0)$ m s^{-1}
Coriolis parameter	f (43°N) = 10^{-4} s^{-1}
Lateral boundaries	Periodic
Bottom boundary	Rigid free-slip
Roughness length	0.1 m

Table 1. General step cooling flux LES characteristics

All simulations were done on a 640 m x 640 m x 640 m domain, similar to previous SBL studies (Basu and Porté-Agel 2006; Kosović and Curry 2000; Saiki et al. 2000; Zhou and Chow 2011). We use tworesolutions. Table 2 shows that we have one run with a horizontal resolution of 8 m and a minimal vertical resolution of 2.5 m [SBL8] and another run with a horizontal resolution of 16 m and a minimal vertical resolution of 5 m [SBL16]. These resolutions may be too coarse for a robust LES, but they should still provide reasonable results (Beare et al. 2006). Furthermore, we seek to understand LASS's abilities to simulate the boundary layer as it cools at a coarse resolution for a later simulation of the transitioning boundary layer. This LES of the transitioning boundary layer will require incorporating larges scales of a CBL as well as the small scales of the SBL, and a grid smaller than 8 m would be cost prohibitive.

Run name	(nx,ny,nz)	Δ_x (m)	Δ_y (m)	AR	Large Δ_t (s)	Small Δ_t (s)
SBL8	(83,83,83)	8	2.5	3.2	0.125	0.0125
SBL16	(43,43,43)	16	5	3.2	0.25	0.025

Table 2. Step Cooling Flux LES run parameters

A constant cooling flux was applied for two hours before it was ramped up to the next surface flux. We sequentially applied four cooling fluxes: -0.005, -0.01, -0.025, and -0.05 K m s^{-1}, which mimic the simulations of Jiménez and Cuxart (2005). A temporal schematic of these cooling fluxes can be found in Figure 1. With this succession of cooling fluxes, we attempted to portray an idealized cooling of a flat, dry area on a clear night.

While we recognize that applying a strong cooling

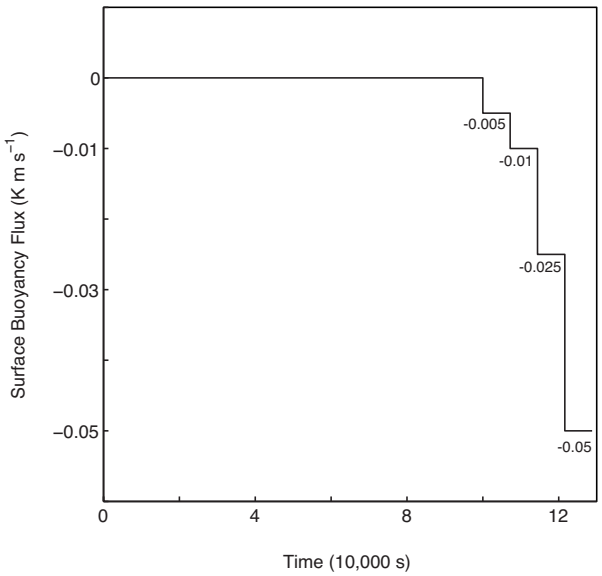

Figure 1. Temporal change of the surface cooling flux. The simulations are initialized with the neutral boundary layer with zero surface cooling/heating for 100,000 s. Constant cooling fluxes are applied in two hour blocks and increase with time.

flux boundary condition, such as - 0.025 and -0.05 K m s^{-1}, can lead to unexpected results because of the dual nature of this boundary condition (Basu and Porté-Agel 2006; Mahrt et al. 1994; Malhi 1995), we still apply it for two reasons: 1) we would like to confirm that runaway cooling with high surface cooling fluxes does occur when using LASS; 2) we plan to use a surface flux boundary condition to simulate the transition of a CBL to a weak SBL.

3.2 *Results*

Mean and turbulent results are from the end of the two hour cooling blocks, unless specified. For convenience, we reset the time at the onset of cooling and refer to time after this onset as cooling time.

3.2.1 *Vertically Integrated Turbulent Kinetic Energy*

Since the resolution of our simulations is coarse, we check if LASS can sustain resolved turbulence or if the flow laminarizes. We use the vertically integrated resolved turbulent kinetic energy [TKE] to gauge the turbulence at an instance. The neutral boundary layer initialization provided plenty of turbulence, but cooling of the boundary layer quickly damped the resolved TKE [Figure 2]. Episodes of enhanced turbulence, where the vertically integrated TKE spikes, can be seen during the first two cooling flux blocks. According to Cederwall (2001), at those cooling fluxes with a geostrophic wind of 10 m s^{-1}, continuous and enhanced turbulence should be observed. The conditions of the third cooling flux [-0.025 K m s^{-1}] fall close to a zone where enhanced turbulence is reduced, but turbulence is sustained. The SBL8 simulation appears to sustain the resolved

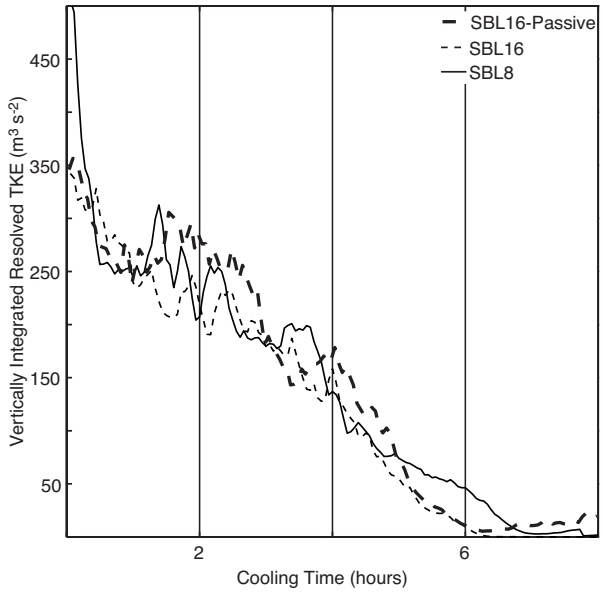

Figure 2. Vertically Integrated Turbulent Kinetic Energy for the SBL8, SBL16, and SBL16- Passive.

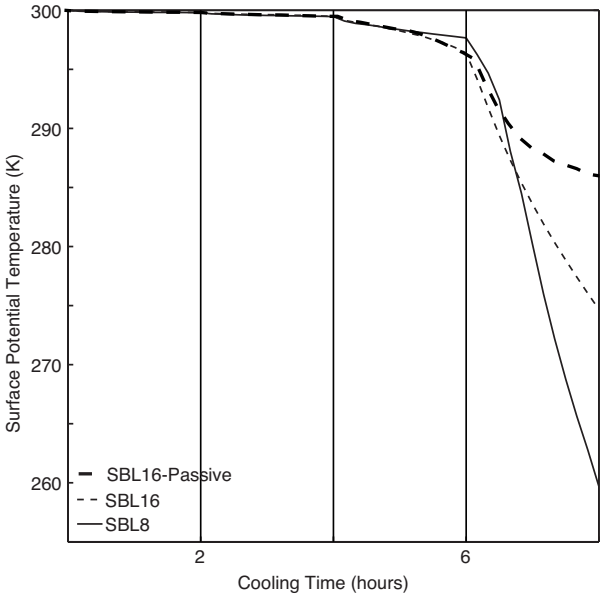

Figure 3. Temporal change of the surface potential temperature. Constant cooling fluxes are applied in two hour blocks and increase with time.

turbulence and have some smaller episodes of enhanced turbulence, but SBL16 cannot sustain the resolved turbulence. SBL8 quickly laminarizes once the strongest cooling flux [-0.05 K m s^{-1}] is applied. Jiménez and Cuxart (2005) explained that the strong cooling of -0.05 K m s^{-1} may be an unrealistic boundary condition, and is probably the reason we see the laminarization and runaway cooling at the surface.

3.2.2 *Temperature Evolution*

Figure 3 shows the evolution of the surface temperature with cooling for SBL8 and SBL16. For the weak surface cooling periods, -0.005 and -0.01 K m s^{-1}, the results are similar and are not affected by resolution. However, with an increased cooling flux we see that the solutions begin to disagree. For the largest cooling flux, we also see that the simulations suffer from runaway cooling. SBL8 cools, on average, at a calculated rate of ~ 19 K h^{-1} and SBL16 cools, on average, at a slower rate of 10 K h^{-1}. In addition, we ran a special case of SBL16, in which we used the passive version of LASS. This version removes the SGS buoyancy term in the SGS stress model. The passive and active versions of LASS appear to agree up until the application of the strong cooling flux. This plot and the TKE values of ~ 20 m^3 s^{-2} in the last cooling block indicate that the passive version of SBL16 was able to sustain turbulence even with this strong cooling. The average cooling rate for this period slowed down to 5 K h^{-1}. The added buoyancy term may have accelerated the destruction of resolved TKE.

The development of the potential temperature in the domain for SBL8 can be seen in Figure 4. The lines represent the temperature profile and are spaced every

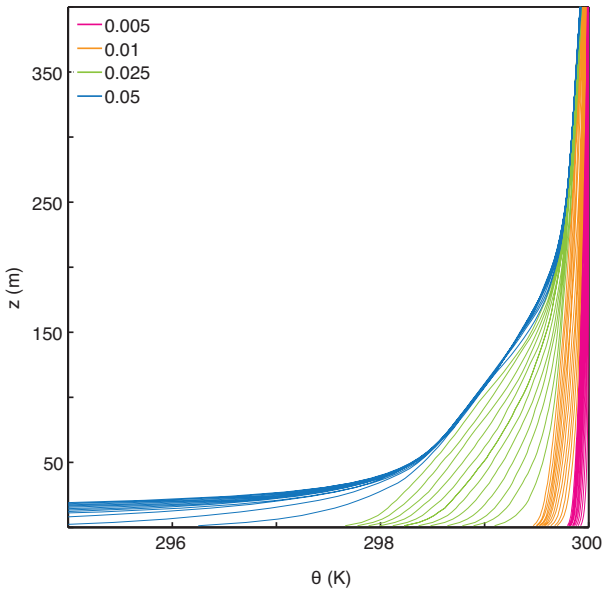

Figure 4. Temporal change of the potential temperature. Constant cooling fluxes are applied in two hour blocks and increase with time. Lines are spaced at 600 s. The profiles move from right to left with time.

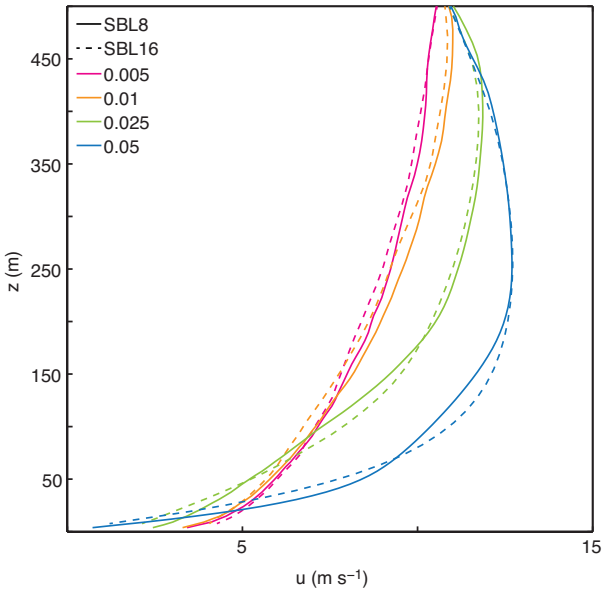

Figure 5. Resolved horizontal velocity component *u* for SBL8 and SBL16 at the end of the cooling flux periods.

600 s. The development of the profiles appears reasonable for a given cooling flux (except for the very strong cooling case of -0.05 K m s^{-1}). The surface cools along with some of the air aloft. The profiles also show that the abrupt transition from one cooling flux to another affects the profiles much more than continuous cooling at the same flux.

3.2.3 *Velocity Profile*

The development of the velocity profiles is affected by the increased cooling fluxes [Figure 5]. As the cooling fluxes increase in magnitude, the maximum of the velocity in- creases, shear is elevated, and a low-level jet begins to appear. Additionally, SBL8 and SBL16 produce similar velocity profiles at each instant in time. Larger discrepancies exist at higher cooling fluxes. However, at these cooling fluxes, we believe that SBL8 and SBL16 eventually laminarize. The velocity profiles trends are similar to the trends for a case in Jiménez and Cuxart (2005). Their plotted profiles had an 8 m s^{-1} geostrophic wind, but the same cooling flux scheme.

3.2.4 *SGS Turbulence Anisotropy*

Since the vertical motions are damped by the stable stratification, the turbulence should be anisotropic. Few SGS turbulence models can provide this one property. The six SGS stresses create a stress tensor. By solving for the eigenvalues of each tensor, we can see the directional preference of the stresses. The x-axis will tell you the shape, or how many directions are dominant. Pancake has two components (left side), rod is towards one (right side), and sphere, has all three components, x,y,z (isotropic), dominant. For more details, the reader is encouraged to refer to Pope (2000). As we shift towards the upper corners of the triangle, the intensity of the dominance of one or two components increases. At the end of the second cooling period, the SBL8 and SBL16 anisotropy characteristics are similar to those in the neutral boundary layer [NBL], as can be seen in

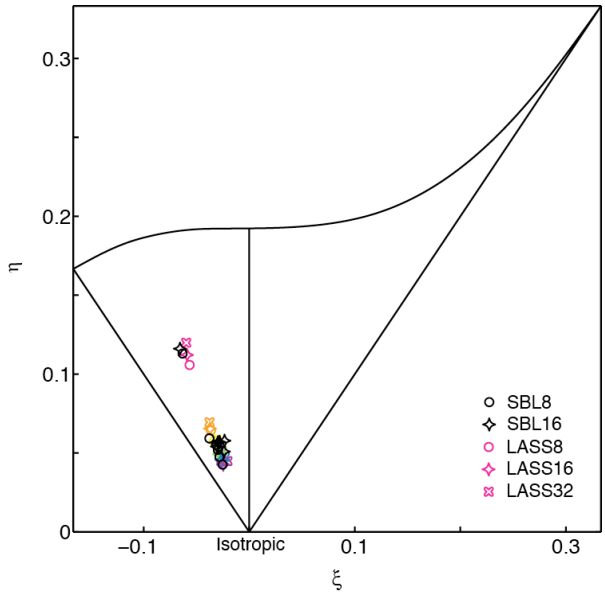

Figure 6. Lumley triangle of the LASS SGS stress anisotropy tensors. Colors symbolize the SGS anisotropy at the six points nearest to the surface for an equivalent neutral boundary layer. The red shapes are closest while the violet shapes are furthest from the surface. Data at the end of second cooling period [4 hours of cooling] of -0.01 K m s^{-1} are shown in black.

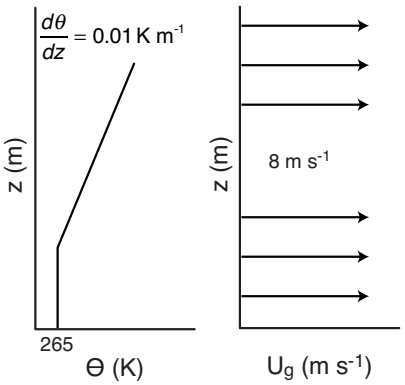

Figure 7. Initial profiles of the potential temperature and the x component of the geostrophic wind velocity, U_g, for the simulated GABLS cases.

Figure 6. The plotted points nearest to the wall are in the middle of the diagram, while those farthest away approach the origin. Thus, the anisotropy decreases with distance from the wall and, being on the left side of the triangle, indicates pancake shaped eddies. The grid anisotropy here is approximately 3 as it was for the NBL. For NBL simulations, we found that grid anisotropy has a large effect on the apparent turbulence anisotropy (Enriquez, 2013). Given that caveat, it appears that for this simulation, the anisotropy of the SGS stresses is not affected by the stratification.

4. INTER-COMPARISON OF LES MODELS WITH THE GLOBAL ENERGY AND *WATER CYCLE EXPERIMENT ATMOSPHERIC BOUNDARY LAYER STUDY (GABLS)*

Now that we have examined how LASS behaves under different cooling fluxes, we examine how LASS performs in a moderately stable case. The case chosen is based on Arctic observations and was simulated by Kosović and Curry (2000), and was later simulated with a variety of LES turbulence models by Beare et al. (2006).

Domain height, H	400 m
Domain width x length	400 m x 400 m
Reference temperature	265 K
Geostrophic wind	$(U_g, V_g) = (8, 0)$ m s^{-1}
Coriolis parameter	f (43°N) = 1.39 x 10^{-4} s^{-1}
Lateral boundaries	Periodic
Bottom boundary	Rigid free-slip
Roughness length	0.1 m
Damping layer	Above 300 m

Table 3. General GABLS LES characteristics

Our simulations follow the details of Beare et al. (2006) and are initialized with a constant geostrophic wind of 8 m s^{-1} at a latitude of 73°N. At this latitude, the Coriolis parameter, f, is 1.39 x 10^{-4} s^{-1}. We set the potential temperature to 265 K, from the ground to 100 m, and then linearly increase it to 268 K. All simulations are done on a 400 m x 400 m x 400 m domain. The surface fluxes are computed with a stability-dependent drag coefficient using Monin-Obukhov similarity theory and a roughness length of 0.1 m. Initial conditions of the simulation can be seen in Figure 7 and general LES parameters are listed in Table 3. Instead of a cooling flux, a cooling rate of 0.25 K h^{-1} is applied for eight hours. Table 4 shows that we have one run with a horizontal resolution of 12.5 m and a minimal vertical - resolution of 6.25 m and a minimal vertical resolution of 1.95 m.

Run name	(nx,ny,nz)	Δ_x (m)	Δ_y (m)	AR	Large Δ_t (s)	Small Δ_t (s)
GABLS 12.5	(35,35,35)	8	12.5	3.9	0.125	0.0125
GABLS 6.25	(67,67,67)	16	6.25	1.95	0.25	0.025

Table 4. GABLS LES run parameters

4.1 *LES Results*

Simulations are carried out over for eight hours and data presented is averaged over the last hour. The 12.5 m, 6.25 m, and 2 m data from Beare et al. (2006) used for comparison can be found at: http://gabls.metoffice.com/lem_data.html.

We present the vertical profiles of wind speed and potential temperature for the two GABLS runs, along with the Beare et al. (2006) data in Figure 8. In general, the profiles exhibit a noticeable super-geostrophic jet near the top of the boundary layer and a positive curvature in the potential temperature. These common characteristics are also portrayed in Beare et al. (2006); Huang and Bou-Zeid (2013). For a given resolution, the LASS simulation falls within the spread of the Beare et al. (2006) data. The LASS model runs tend to predict slightly higher potential temperatures right above the surface than the other LES runs.

As the resolution increases, we see 1) that the jet becomes more evident and that the peak shifts towards the ground and 2) the potential temperature decreases slightly by the surface, and increases towards the top of the domain. The main difference between the two runs is seen in the wind speed profiles. In particular, the profile at the top of the boundary layer is the most changed. For a LES that used a turbulence model that provided backscatter, Beare et al. (2006) also showed that as resolution increased there was a general decrease in the height of the jet, along with an increase in the jet strength. Backscatter was used to explain the boundary layer depth enhancement for the coarser resolutions. This trend in LASS may also be due to backscatter since the inclusion of buoyancy in our model allows backscatter because of the interaction between the buoyancy, production, and dissipation terms.

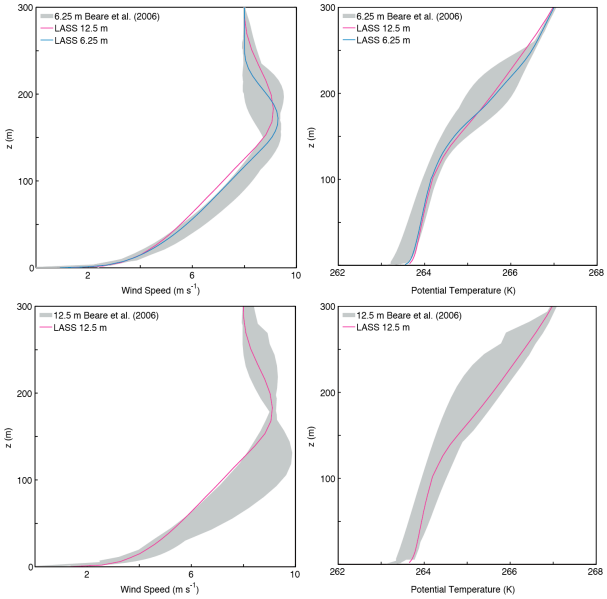

Figure 8. LES wind speed and potential temperature profiles at 12.5 m resolution (top). Comparison of LES wind speed profiles at 6.25 m resolution (bottom). Each profile is compared with the corresponding Beare et al. (2006) data.

We also compare our 12.5 m and 6.25 m resolution profiles with the 2 m data of Beare et al. (2006), which can be seen in Figure 9. They concluded that a resolution of 3.125 m or less is ideal for simulating a moderately SBL, while reasonable behavior can still be obtained with a resolution of 6.25 m. Our results here, confirm their findings. While, the 12.5 m resolution run does not capture the low-level jet as well as the 2 m resolution runs, the 6.25 m run appears to do quite well. It predicts the stronger and lower jet. The potential temperature profile provided by the 6.25 m run fits the 2m data much better than the 12.5 m run, confirming our previous experience (Enriquez 2013) with LASS - that it is able to resolve structures that are about the same size as those resolved with a Dynamic Wong-Lilly simulation at twice the resolution.

5. CONCLUSIONS

We showed that LASS can adapt very well to stable conditions and adequately simulate the stable boundary layer. Simulations of the weakly stable boundary layer showed episodes of enhanced turbulence and a simulation of the moderately stable boundary layer produced an enhanced low-level jet. It was also shown that LASS can provide suitable wind speed profiles at a much coarser resolution.

Simulations of the stable boundary layer with a coupled atmosphere-land surface model may be the next appropriate method of assessing LASS. Under these conditions, we could compare simulation results with analytical profiles and field data.

6. ACKNOWLEDGMENTS

We appreciate our helpful discussions with Professor Tina Chow and Dr. Bowen Zhou of UC Berkeley and Dr. Peter Sullivan of NCAR. We are grateful to NCAR for the computing time used in this research, research support from the NSF Grant 1001262, and travel support from a Newton International Fellowship from The Royal Society.

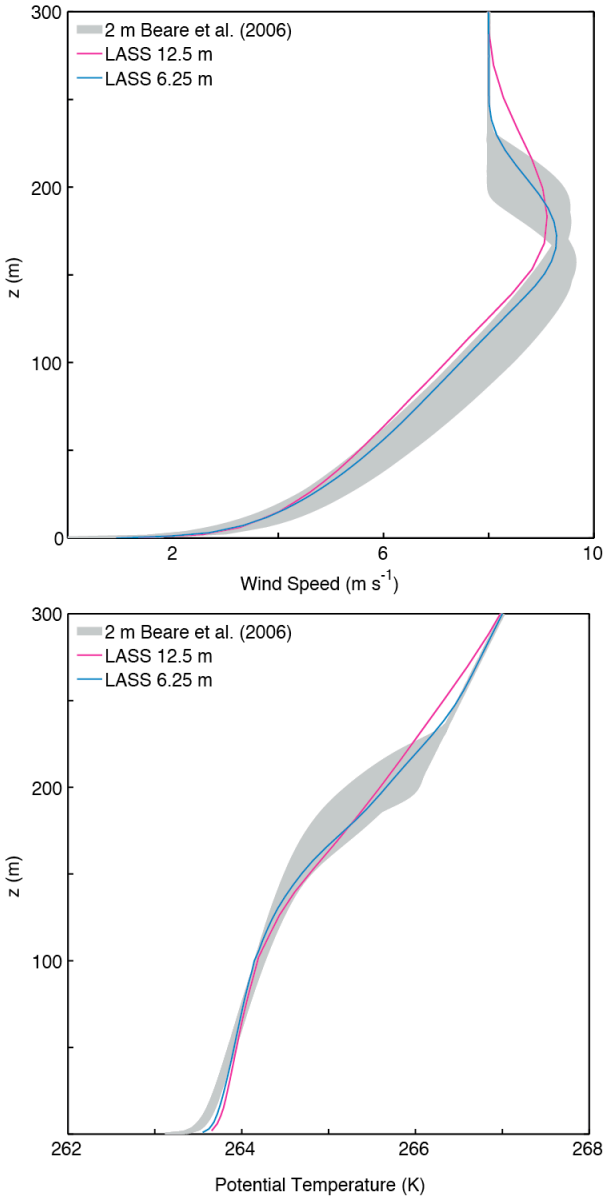

Figure 9. Comparison of LES wind speed (top) and potential temperature (bottom) profiles at 12.5 m and 6.25 m resolutions with Beare et al. (2006) 2 m data.

7. REFERENCES

Basu, S., and F. Porté-Agel, 2006: Large-eddy simulation of stably stratified atmospheric boundary layer turbulence: A scale-dependent dynamic modeling approach. *Journal of the Atmospheric Sciences*, **63,** 2074-2091.

Beare, R., and Coauthors, 2006: An intercomparison of large-eddy simulations of the stable boundary layer. *Boundary-Layer Meteorology*, **118,** 247-272.

Cederwall, R. T., 2001: Large-eddy simulation of the evolving stable boundary layer over flat terrain, Dissertation, Stanford University.

Enriquez, R. M., 2013: Subgrid-scale turbulence modeling for improved large-eddy simulation of the atmospheric boundary layer, Dissertation, Stanford University.

Huang, J., and E. Bou-Zeid, 2013: Turbulence and Vertical Fluxes in the Stable Atmospheric Boundary Layer. Part I: A Large-Eddy Simulation Study. *Journal of the Atmospheric Sciences*, **70,** 1513-1527.

Jiménez, M. A., and J. Cuxart, 2005: Large-Eddy Simulations of the Stable Boundary Layer Using the Standard Kolmogorov Theory: Range of Applicability. *Boundary-Layer Meteorology*, **115,** 241-261.

Kosović, B., and J. A. Curry, 2000: A Large Eddy Simulation Study of a Quasi-Steady, Stably Stratified Atmospheric Boundary Layer. *Journal of the Atmospheric Sciences*, **57,** 1052-1068.

Mahrt, L., J. Sun, D. Vickers, J. I. Macpherson, J. R. Pederson, and R. L. Desjardins, 1994: Observations of Fluxes and Inland Breezes over a Heterogeneous Surface. *Journal of the Atmospheric Sciences*, **51,** 2484-2499.

Malhi, Y., 1995: The significance of the dual solutions for heat fluxes measured by the temperature fluctuation method in stable conditions. *Boundary-Layer Meteorology*, **74,** 389-396.

Pope, S. B., 2000: *Turbulent Flows.* Cambridge University Press.

Saiki, E. M., C.-H. Moeng, and P. P. Sullivan, 2000: Large-Eddy Simulation Of The Stably Stratified Planetary Boundary Layer. *Boundary-Layer Meteorology*, **95,** 1-30.

Yoshizawa, A., 1986: Statistical theory for compressible turbulent shear flows, with the application to subgrid modeling. *Physics of Fluids*, **29**, 2152.

Zhou, B., and F. K. Chow, 2011: Large-eddy simulation of the stable boundary layer with explicit filtering and reconstruction turbulence modeling. *Journal of the Atmospheric Sciences*, **68,** 2142-2155.